

# Systematic Method for Thermomechanically Consistent Coarse-Graining: A Universal Model for Methacrylate-Based Polymers

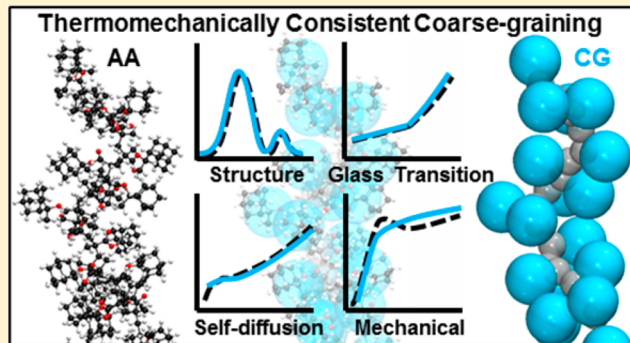
David D. Hsu,<sup>†</sup> Wenjie Xia,<sup>‡</sup> Steven G. Arturo,<sup>§</sup> and Sinan Keten\*,<sup>†,‡</sup>

<sup>†</sup>Department of Mechanical Engineering, Northwestern University, 2145 Sheridan Road, Evanston, Illinois 60208-3109, United States

<sup>‡</sup>Department of Civil & Environmental Engineering, Northwestern University, 2145 Sheridan Road, Evanston, Illinois 60208-3109, United States

<sup>§</sup>Core Research & Development, The Dow Chemical Company, 400 Arcola Road, Collegeville, Pennsylvania 19426, United States

**ABSTRACT:** We present a versatile systematic two-bead-per-monomer coarse-grain modeling strategy for simulating the thermomechanical behavior of methacrylate polymers at length and time scales far exceeding atomistic simulations. We establish generic bonded interaction parameters via Boltzmann inversion of probability distributions obtained from the common coarse-grain bead center locations of five different methacrylate polymers. Distinguishing features of each monomer side-chain group are captured using Lennard-Jones nonbonded potentials with parameters specified to match the density and glass-transition temperature values obtained from all-atomistic simulations. The developed force field is validated using Flory–Fox scaling relationships, self-diffusion coefficients of monomers, and modulus of elasticity for p(MMA). Our approach establishes a transferable, efficient, and accurate scale-bridging strategy for investigating the thermomechanics of copolymers, polymer blends, and nanocomposites.



## 1. INTRODUCTION

Methacrylate based polymers are ubiquitously used in manufacturing thin films, nanocomposites, and nanoelectronics because they give rise to processable materials with remarkable mechanical properties.<sup>1–4</sup> The thermal, optical, and electrical characteristics of methacrylate polymers can also be fine-tuned using copolymers at varying compositions.<sup>5–7</sup> Due to their high transparency and dissolution in solvents, methacrylate homopolymer- and copolymer-based thin films are increasingly being used in the design of microsensors and lithographic manufacturing of semiconductor devices.<sup>1,8–10</sup> As industrial applications call for greater mechanical performance and smaller material dimensions in devices, it becomes progressively vital to accurately predict material characteristics at the nano- and molecular-scales and low-molecular weights via simulation. Computational methods aimed at addressing this issue must capture specific chemistry of monomers, interfacial and phase behavior, and molecular weight effects with a manageable number of model parameters for ease of use.

Molecular dynamics simulations (MD) provide crucial insight into the molecular mechanisms underpinning molecular mobility, glass-transition temperature, and mechanical property gradients near nanoscale interfaces.<sup>11–13</sup> Even though all-atomistic MD simulation is fairly accurate in capturing nanoscopic features, it has yet to emerge as a rapid design tool capable of bottom-up characterization and prediction for polymer materials. Spatiotemporal limitations of all-atom MD make it challenging to simulate the physics of polymers in

nanostructures, such as thin films, that are on the order of tens of nanometers over time-scales relevant to polymer dynamics. The onset of glass-transition, diffusion, or copolymer phase segregation behavior are particularly challenging to address via simulation.<sup>12–16</sup> Reduced order models such as coarse-grained molecular dynamics (CGMD) techniques alleviate the scale limitations of all-atom MD by systematically extracting data from atomistic structures and reducing groups of atoms into coarse-grain beads called “superatoms”.<sup>17–19</sup> These CG models are computationally efficient due to the reduced number of degrees-of-freedom, simpler potential functions, longer simulation time-steps, and accelerated dynamics. This enables simulations of longer length and time-scale phenomena and also improves the statistical sampling of the system phase space.<sup>17,20</sup> Some systematical approaches can also conserve select features such as thermodynamic properties, conformational and distance distributions, tacticity, as well as other aspects, providing semiquantitative predictive capabilities.<sup>21–24</sup> However, in most CG studies, a mapping is performed based on atomistic simulations for a single homopolymer type under narrow temperature boundaries.<sup>18,24</sup> Major challenges in the way of generalized coarse-grained force fields for polymers include (i) the difficulty to simultaneously retain chemical, mechanical, structural, and dynamical properties in the up-scaling process, (ii) limited transferability due to diversity of

Received: February 1, 2014

Published: April 8, 2014

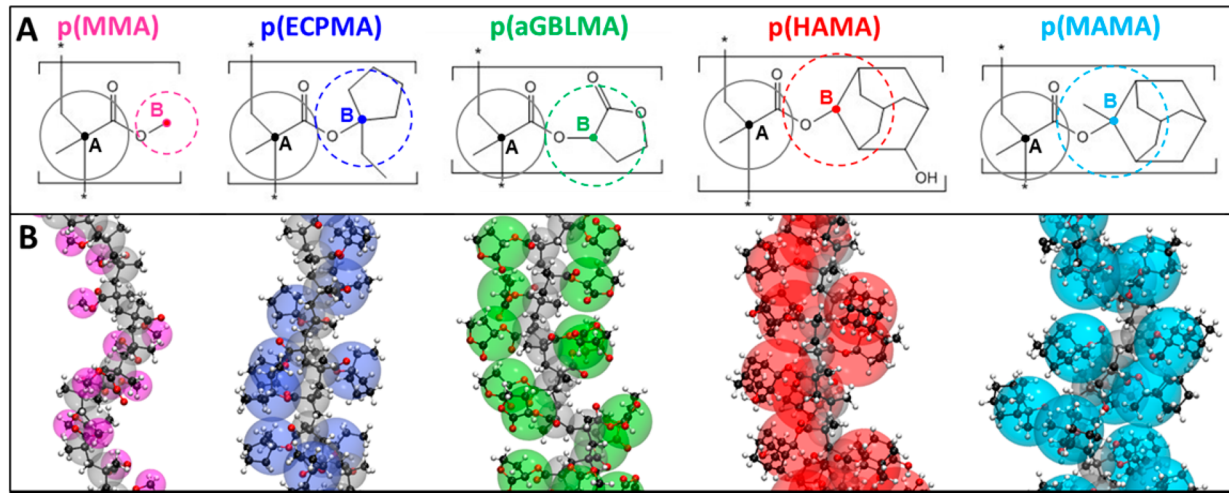


**Figure 1.** (A) Polymer structure and coarse-grain bead center locations chosen for p(MMA), p(ECPMA), p(aGBLMA), p(HAMA), and p(MAMA). (B) For the two-bead per monomer CG system, each repeat monomer is considered as two groups, a methacrylate backbone group and a side-chain group. Backbone coarse-grain bead is shown in gray, and side-chain bead is color coordinated.

monomer chemistry in engineered polymers, and (iii) limitations of predictive power beyond the quantities of interest that are used in model calibration. Conversely, in biomolecular systems such as proteins, some coarse-grain models have been systematically developed in such a way as to be generalizable over multiple systems and applications without the need for full reparametrization. This requires identification of universal and diverse features of the monomers involved, such as parametrizations of the common backbone features of most amino acids and their distinctive side-chain groups as done in the widely used MARTINI and GROMOS force fields.<sup>25,26</sup> However, for both biological and synthetic polymers, accurately capturing the static and dynamic attributes that control the thermomechanical behavior of soft materials (glass-transition, elastic properties, self-diffusion behavior, etc.) has not been a major focus.

As a step toward acquiring this capability for methacrylate-based polymers, here we present a systematic coarse-graining method that illustrates a strategy for capturing the physical properties of different methacrylate polymers. The selected methacrylates are particularly suited for coarse graining because of their common backbone structure and distinct side groups. This allows us to model the backbone using a simple universal two-bead CG model with consistent bead force centers and common potentials for bonded terms. We then model the side group behavior with unique pairwise Lennard-Jones potential parameters representing the side-chain mass, bulk, and chemical functionality. This new strategy provides solutions to the aforementioned issues related to scale bridging, namely, identification of universal and diverse features of monomers, transferability of parameters within a subclass of polymers (i.e., methacrylates), and matching of thermomechanical properties, including predictive capability of features that the model is not originally calibrated for. We demonstrate the applicability of the model using five different monomers with distinctly different side-chain chemistries involving bulky pendant groups, polar functionalities, and hydrogen bonding. The strategic choice of force centers facilitates simple extensions of the force field to study more complex systems such as copolymers.<sup>27–31</sup>

The outline of this paper is as follows. First, we describe the systematic coarse-graining methodology for obtaining bonded and nonbonded interactions. Next, we present how dynamic

and thermomechanical properties can be matched through adjustment of certain nonbonded potential parameters, particularly focusing on diffusion and glass-transition metrics. Finally, we present validations of the model through dynamic and mechanical property mapping and comparison with Flory–Fox relationships and elastic constants obtained from all-atom simulation results and experiments.

## 2. COARSE-GRAINING STRATEGY AND MONOMER LIBRARY

Our coarse-graining approach is based on the strategy of using two-beads per methacrylate monomer to simplify the structural and chemical representation of the all-atom system. The methacrylate homopolymers used in the coarse-graining are as follows: poly(methyl methacrylate) p(MMA), poly(1-ethylcyclopentyl methacrylate) p(ECPMA), poly( $\alpha$ - $\gamma$ -butyrolactone methacrylate) p(aGBLMA), poly(3-hydroxyl-1-adamantyl methacrylate) p(HAMA), and poly(2-methyl-2-adamantyl methacrylate) p(MAMA). These monomers are chosen as a representative group that have the most variety in chemical structure and are commonly used in thin films and photoresist materials, for which coarse-grained simulations would offer the possibility to elucidate molecular mechanisms governing the thermomechanical stability of nanostructures. Altogether, these monomers provide considerable chemical diversity to test whether the coarse-graining approach can be transferable to unique chemical modifications despite structural and molecular weight similarities. In particular, p(HAMA) and p(MAMA) both have bulky adamantyl side-chain structure with similar molecular weight; however, they exhibit quantitatively dissimilar thermomechanical behavior due to hydrogen bonding effects in p(HAMA) that are absent in p(MAMA). Likewise, p(ECPMA) and p(aGBLMA) have similar molecular weight. P(aGBLMA), however, also exhibits dissimilar thermomechanical behavior as compared to P(ECPMA) due to highly polar interactions in the former homopolymer. P(MMA), which has a methyl side-chain group, is included as a baseline monomer structure. (See Figure 1.)

In order to determine both the universal and unique parameters for methacrylates, the all-atom systems for the five different methacrylate homopolymers must first be

generated. Each atomistic model is generated with 4 chains, 75 monomers per chain, and is initially built using Accelrys Materials Studio. The resulting systems with all periodic boundary conditions are then relaxed using the LAMMPS open source MD package developed by Sandia National Laboratories.<sup>32</sup> The general-purpose Dreiding force field<sup>33</sup> is employed for all-atomistic bulk systems. To relax the system, the energy is minimized using the conjugate gradient algorithm.<sup>34</sup> Two annealing cycles from 210 to 750 K are performed, and then the system is further equilibrated for an additional 2 ns at 750 K under the NPT ensemble using a Nose-Hoover barostat that maintains the pressure at 1 atm with a time step  $\Delta t = 1$  fs. We use the convention that the temperature damping parameter  $T_{damp}$  is set as 100 times  $\Delta t$ , which in our case  $T_{damp} = 100$  fs, and we use  $P_{damp}$  set to 1000 fs. The final equilibrated configurations are cooled to 300 K and are used to develop the CG parameters which take inputs from subsequent simulations.

**2.1. Atom Center Definition.** Once the atomistic system has been simulated, the coarse-grained model is generated to reproduce the structural and dynamic properties of the atomistic simulation. For the two-bead per monomer CG system, each repeat monomer is defined as two groups. (See Figure 1.) The first group, denoted as type “A”, represents the methacrylate group ( $C_4O_2H_5$ ) forming the connected polymer chain backbone. This choice is consistent across all of the five homopolymers in focus. The backbone “A” bead centers are located at the quaternary carbon atoms in the methacrylate group. The second, type “B” side-chain group, represents the specific side-chain groups that depend on the homopolymer type. “B” bead centers are centered at the first side-chain carbon atom bound to the ester single bonded oxygen. These choices allow us to maintain consistent bead center locations for all of the methacrylate-based polymer types regardless of side-chain structure. This approach minimizes the number of parameters that would be needed to define the AB bond length and AAB angle in *homo-* and *co*-polymers. Therefore, the parameters are much more transferable across different types of monomers compared to other approaches, such as models where the side-chain “B” bead center is defined to be the center of mass of the side-chain.

**2.2. Bonded Interaction Definition.** Backbone AA bonds are defined as the effective bonds that connect adjacent type “A” methacrylate backbone groups, and AB bonds are defined to connect each “A” backbone group to its adjacent “B” side-chain group. These bond definitions are advantageous because they allow for consistent bonded interaction parameters as well as identical nonbonded interactions for the backbone of each methacrylate-based polymer. AAA angles describe the angle between three adjacent backbone beads, and similarly, AAB angles are defined as the forward and backward angles between two adjacent backbone beads and a connected side-chain bead. The backbone angles and torsions help control the stiffness of the polymer. AAAA torsions are defined between four adjacent backbone beads and last, BAAB torsions are defined between two adjacent backbone beads and their attached side-chains. With these definitions, the distributions and main features of the polymer chains are adequately captured, as such AAAB and BAAA torsional angles are not defined.

**2.3. Nonbonded Interaction Definition.** Lennard-Jones nonbonded potential interactions are defined between backbone beads (AA), between backbone beads and side-chain beads (AB), and also between side-chain beads (BB). Along the coarse-grain chain, the nonbonded interactions are turned off

for nearest neighbors and next nearest neighbors but are turned on for third nearest neighbors and all other beads further along the chain. Note that “nearest neighbors” refers to bond order and not radial distance. This allows adjacent side-chain beads to interact via nonbonded (BB) forces. Here we aim to reproduce the effects of polar interactions and hydrogen-bonding on select thermomechanical properties through Lennard-Jones interactions, without explicit charge definition in the coarse grain model.

#### 2.4. Coarse-Grained Molecular Dynamics Simulations.

To optimize the bonded potential parameters, we use a coarse-grain system with 5 chains, 100 monomers per chain, and 2 beads per monomer, for a total of 1000 beads. Although the chains are relatively short, bonded parameters are mostly based on intrachain and short length scale vibrational modes of the bulk system, which are not strongly affected by the chain length. Nonbonded parameters, however, are based on glass transition behavior, which is affected by the chain length. This is evidenced by the ability for the model to match  $T_g$  behavior over a range of molecular weights using the Flory–Fox relation. The chains are placed using a random walk algorithm into a cubic simulation box with periodic boundary conditions on all sides. After a minimization step, chains are pushed apart to remove close contacts by slowly turning on a soft, purely repulsive potential in the NVT ensemble at 300 K using the Nose-Hoover thermostat with a time step  $\Delta t = 4$  fs. Again, using the convention  $T_{damp}$  equals 100 times the time step  $\Delta t$ , we set our  $T_{damp}$  to 400 fs in the CG model for all simulations. Subsequently, the system undergoes an annealing step where the temperature is ramped from 300 to 750 K over 0.4 ns, the system is held at the elevated temperature at 750 K for 8 ns, and then is cooled back down to 300 K under the NVT ensemble over 0.4 ns. Finally, the simulation box is subjected to a high pressure (1000 atm) over 4 ns at 300 K to compress the system to a converged density under the NPT ensemble using the Nose-Hoover barostat with  $T_{damp} = 400$  fs and  $P_{damp} = 1000$  fs. We release this high pressure condition and allow the system to equilibrate to its native density over a period of 8 ns in the NPT ensemble.

**2.5. Bonded Interaction Optimization.** Here we give an overview of the process used to insert atomistic detail into the CG model which is based on the Inverse Boltzmann Method (IBM).<sup>17,22,35</sup> Once the bead center locations have been established, the initial bond lengths, angles, dihedrals, and nonbonded potentials are calculated from the bonded and nonbonded distributions. Unlike earlier studies that have coarse grain models focused on a single type of monomer,<sup>20,28,36–39</sup> here we define our target bonded distributions as the average probability density across the five different methacrylate homopolymer systems. The average potentials for bond-stretching, angles, and dihedrals follow the formulas

$$\bar{U}_{bond}(l) = \frac{1}{N} \sum_{i=1}^N [-k_b T \ln(P_i(l))] \quad (1)$$

$$\bar{U}_{angle}(\theta) = \frac{1}{N} \sum_{i=1}^N [-k_b T \ln(P_i(\theta))] \quad (2)$$

$$\bar{U}_{dihedral}(\phi) = \frac{1}{N} \sum_{i=1}^N [-k_b T \ln(P_i(\phi))] \quad (3)$$

where  $k_b$  is the Boltzmann constant,  $T$  is the temperature,  $P_i$  is the probability distribution as a function of bond lengths  $l$ , angles  $\theta$ , and dihedral angles  $\phi$  for each of the  $N = 5$  different polymers, p(MMA), p(ECPMA), p(aGBLMA), p(HAMA), and p(MAMA). The resulting effective average potentials are then fit with analytical potentials of the following forms:

$$U_{CGbond}(l) = k_{bond}(l - l_0)^2 \quad (4)$$

$$U_{CGangleAAA}(\theta) = -k_b T \ln \left[ a_1 \exp\left(-\frac{\theta - \theta_1}{b_1}\right)^2 + a_2 \exp\left(-\frac{\theta - \theta_2}{b_2}\right)^2 \right] \quad (5)$$

$$U_{CGangleAAB}(\theta) = k_2(\theta - \theta_0)^2 + k_3(\theta - \theta_0)^3 + k_4(\theta - \theta_0)^4 \quad (6)$$

$$U_{CGdihedral}(\phi) = \sum_{k=1}^5 A_k \cos^{k-1}(\phi) \quad (7)$$

The AA and AB bond stretching lengths are fit with eq 4, where  $k_{bond}$  is a constant in energy units and  $l_0$  is the equilibrium bond length. The AAA angle potential is fit with an inverted double Gaussian eq 5 where  $a_1$ ,  $b_1$ ,  $a_2$ , and  $b_2$  are constants,  $k_b$  is the Boltzmann constant,  $T$  is the temperature, and  $\theta_1$  and  $\theta_2$  are the two equilibrium angles. The AAB effective potential is fit with a fourth order polynomial function eq 6 where  $k_i$  are constants in energy units per rad<sup>i</sup>, and  $\theta_0$  is the equilibrium angle. Dihedrals AAAA and BAAB are fit with a multiharmonic potential of the form from eq 7, where  $A_k$  are constants in energy units.

Direct implementation of the first Boltzmann inversion estimate for the bonded potentials typically does not give perfectly matching correlations between the CG and all-atom distributions. This is due to some degree of interaction and interdependence between the individual bonded and non-bonded potentials in the CG model, which are calculated independently in the parametrization procedure.<sup>16</sup> Thus, we optimize the CG model iteratively to improve the correlation of the CG distributions with the averaged atomistic target distributions. This is done by incrementally performing Boltzmann iterations on bonded potential terms in the order of decreasing energy contributions. In our case, we use the following sequence of potential optimization stages:  $U_{bond} \rightarrow U_{angle} \rightarrow U_{nonbonded} \rightarrow U_{dihedral}$  as proposed by Reith et al.<sup>39</sup> For example, we begin by optimizing the  $U_{bond}$  potential. Bond length distributions are captured from equilibration simulations with  $U_{angle}$ ,  $U_{nonbonded}$ , and  $U_{dihedral}$  potentials turned off. Once  $U_{bond}$  is fully optimized, we add the  $U_{angle}$  potential to the equilibration simulation and then optimize the  $U_{angle}$  terms without implementing  $U_{nonbonded}$  or  $U_{dihedral}$  potentials. This incremental process is followed until all potential terms have been optimized. If more weakly contributing potential terms are optimized first (i.e.,  $U_{dihedral}$  before  $U_{bond}$ ), stronger potentials will disrupt weak distributions, requiring repetition of optimization efforts. Iterative Boltzmann inversions follow the equations<sup>17,22,35</sup>

$$U_{CGbond}^{n+1}(l) = U_{CGbond}^n(l) + k_b T \ln \frac{P^n(l)}{P^{target}(l)} \quad (8)$$

$$U_{CGangle}^{n+1}(\theta) = U_{CGangle}^n(\theta) + k_b T \ln \frac{P^n(\theta)}{P^{target}(\theta)} \quad (9)$$

$$U_{CGdihedral}^{n+1}(\phi) = U_{CGdihedral}^n(\phi) + k_b T \ln \frac{P^n(\phi)}{P^{target}(\phi)} \quad (10)$$

where  $P^n$  is the probability distribution of the  $n^{\text{th}}$  iteration,  $P^{target}$  is the target distribution,  $U^n$  is the potential function of the  $n^{\text{th}}$  iteration, and  $U^{n+1}$  is the resulting iterated potential function. Generally, the IBM is used to optimize a single CG homopolymer type at a time. In our procedure, we generate five separate CG models for the five methacrylate homopolymer types and simultaneously optimize the average CG distributions for each homopolymer to match the target average CG distribution. Optimization of the nonbonded potential in our case does not use the IBM and is described in detail in the following section.

Distributions at each optimization step for bonded parameters are captured from equilibration simulations which uses the annealed system described in Section 2.4 as a starting point. Bonded potential parameters calculated using eqs 8, 9 or 10 from the previous optimization step are implemented in each new Boltzmann iteration for bonds, angles, or dihedrals, respectively. Chains are gradually pushed apart using a purely repulsive soft nonbonded potential in the NVT ensemble at 300 K with a time step  $\Delta t = 4$  fs and damping parameter  $T_{damp} = 400$  fs. Bond and angle potentials are optimized before the nonbonded Lennard-Jones potential parameters are established. Hence, we equilibrate the system using a purely repulsive potential under the NVT ensemble at 300 K for 8 ns. After the nonbonded potential optimization procedure, the bonds and angles distributions are slightly adjusted to correct for the new pairwise potential. Finally, when dihedral potentials undergo optimization, the purely repulsive nonbonded potential is exchanged for the optimized Lennard-Jones parameters, and all other simulation details remain the same.

**2.6. Nonbonded Potential Parameters.** In our thermo-mechanical mapping approach, the CG model nonbonded parameters are systematically varied to target density, polymer dynamics, and glass-transition properties obtained from atomistic simulations, rather than the radial distribution function (RDF). Here we elect to use the Gromacs-style 12–6 Lennard-Jones (LJ) potential to model the nonbonded interactions between superatoms for its simplicity and computational efficiency in describing nonbonded intra- and intermolecular interactions. We note that any directionality associated with side-chain polar or hydrogen-bonding functionality is lost when using this potential form and thus, it represents a mean-field effect. The nonbonded potential has the following form:

$$U_{nonbond} = 4\epsilon \left[ \left( \frac{\sigma}{r} \right)^{12} - \left( \frac{\sigma}{r} \right)^6 \right] + S_{LJ}(r) \quad (11)$$

Here,  $\sigma$  is the radial distance from the atom where the potential crosses the zero energy line, and  $\epsilon$  is the depth of the well in energy units. This style of the LJ potential provides a smooth transition to zero energy from  $R_{inner} = 12$  Å to  $R_{outer} = 15$  Å by implementing a polynomial function  $S_{LJ}(r)$ . Backbone–backbone AA bead interactions are explicitly defined with two universal parameters  $\sigma_{AA}$  and  $\epsilon_{AA}$ . Side-chain to side-chain interactions are also explicitly defined,  $\sigma_{BB}$ ,  $\epsilon_{BB}$ , and are unique for each homopolymer. Side-chain to backbone bead AB interactions,  $\epsilon_{AB}$  and  $\sigma_{AB}$ , are calculated as the geometric

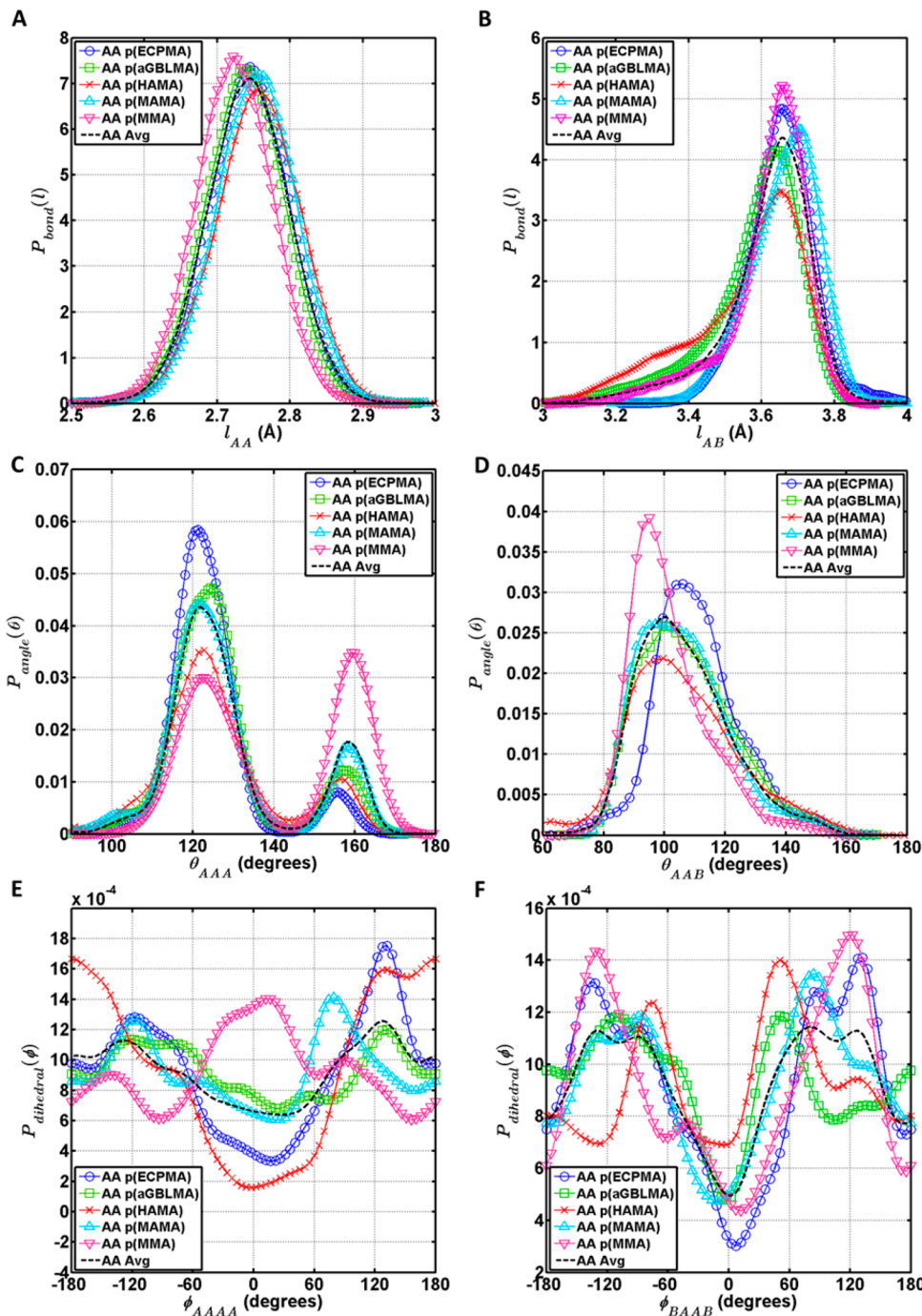


**Figure 2.** All atomistic distributions for five homopolymers. Average over all homopolymers shown as black dotted line. (A) Bond stretching length between two backbone groups (A-A). (B) Effective bond stretching length between the backbone and its corresponding side-chain (A-B). (C) Effective angle between three backbone centers (A-A-A). (D) Effective angle between two adjacent backbone centers and a side-chain (A-A-B). (E) Effective dihedral angle between four backbone centers (A-A-A-A). (F) Effective dihedral angle between adjacent backbone to side-chain bonds (B-A-A-B).

average and arithmetic average, respectively, between the AA and BB parameters. The exception is p(HAMA), which requires further considerations due to its hydrogen bonding capability as discussed below. We use a parametric study to systematically vary  $\epsilon$  and  $\sigma$  values for AA and BB until each individual system matches all-atomistic densities and glass transition temperatures. To accommodate hydrogen bonding effects that occur between the side-chain and backbone groups in p(HAMA), we perform a second parametric study to

systematically vary the  $\epsilon_{AB}$  interaction until both  $T_g$  and the self-diffusion coefficient matches with all-atomistic simulations.

We employ a full factorial Design of Experiments<sup>40</sup> (DOE) to evaluate the sensitivity of  $T_g$  and density to the LJ  $\epsilon$  and  $\sigma$  values and to determine the proper parameters for side-chains and backbone interactions. DOE refers to a systematic method to measure the effect of variations in process variables on a set of key responses. A full factorial DOE requires simulation of every permutation of process variable conditions, which can become computationally intensive unless process variables can

be minimized or coupled. In our case, there are effectively six nonbonded potential parameters for each of the homopolymer systems,  $\epsilon_{AA}$ ,  $\sigma_{AA}$ ,  $\epsilon_{BB}$ ,  $\sigma_{BB}$ ,  $\epsilon_{AB}$ , and  $\sigma_{AB}$ . We are able to reduce the number of DOE process variables to three by using the following steps. Starting with the p(ECPMA) system, we fix the value of  $\epsilon_{AB}$  to be the geometric average between  $\epsilon_{AA}$  and  $\epsilon_{BB}$ , and  $\sigma_{AB}$  is fixed to be the arithmetic average between  $\sigma_{AA}$  and  $\sigma_{BB}$ . We also couple together the  $\sigma_{AA}$  and  $\sigma_{BB}$  values by estimating that  $\sigma_{BB} = \sigma_{AA} + 1 \text{ \AA}$ , which is approximately true for p(ECPMA) based on RDF data obtained from monomer simulations.

We then perform a full factorial DOE with the remaining factors and systematically vary  $\epsilon_{AA}$  and  $\epsilon_{BB}$  from 0.3 to 0.7 kcal/mol in 0.1 kcal/mol increments and  $\sigma_{AA}$  from 4.5 to 6.0 Å in 0.5 Å increments. Using this procedure, we find that the optimal nonbonded parameters for p(ECPMA) are  $\epsilon_{AA} = 0.5 \text{ kcal/mol}$ ,  $\sigma_{AA} = 5.5 \text{ \AA}$ ,  $\epsilon_{BB} = 0.475$ , and  $\sigma_{BB} = 6.57 \text{ \AA}$ . For all other homopolymer systems, we simplify the procedure by using the same  $\epsilon_{AA}$  and  $\sigma_{AA}$  value as obtained for p(ECPMA). This is a reasonable approximation as the "A" backbone chemical structure is identical across all homopolymers. In addition, this approximation is supported from initial DOEs on the other homopolymers which found that the resulting average values were very close to that of p(ECPMA),  $\epsilon_{AA} \sim 0.5 \text{ kcal/mol}$ , and  $\sigma_{AA} \sim 5.2 \text{ \AA}$ . We find that  $\sigma_{BB}$  has a large effect on the density of the system as it governs the excluded volume of the side-chain groups, whereas  $\epsilon_{AA}$  and  $\epsilon_{BB}$  have a negligible effect on the density. Therefore, in our subsequent calibration procedure, we fix  $\epsilon_{BB}$  and vary  $\sigma_{BB}$  to first achieve the target atomistic density of the system. Hence, after adopting  $\sigma_{AA}$  and  $\epsilon_{AA}$  values from p(ECPMA), we do not execute a full DOE for the subsequent systems but rather use a simpler, two-step process: 1) Tune  $\sigma_{BB}$  to achieve the target atomistic density. 2) Tune  $\epsilon_{BB}$  to achieve the target atomistic  $T_g$ .

We note that p(HAMA) requires additional calibration because of hydrogen bonding between the side-chain hydroxyl group and backbone double bonded oxygen. Due to this relatively strong interaction, it is expected that the backbone-side-chain interactions will be higher than backbone or side-chain like interactions. In order to accommodate for any effect on dynamic behavior due to hydrogen bonding, we systematically vary the  $\epsilon_{AB}$  value from 1.5 to 3.5 kcal/mol in 0.3 kcal/mol increments until the diffusion coefficient for coarse-grain HAMA monomers matches with all-atomistic results. In this case, the increase in  $\epsilon_{AB}$  is not found to cause any discernible shift in  $T_g$ .

To measure  $T_g$  in the calibration process, we use the methodology described by Tsige and Taylor.<sup>41</sup> We start with the relaxed polymer system from the steps outlined in Section 2.4 and then implement the Lennard-Jones nonbonded potential parameters. The system is then equilibrated under the NPT ensemble at 210 K for 8 ns using a 4 fs time step to ensure the box dimensions converge to the 210 K density.  $T_{damp}$  and  $P_{damp}$  are maintained at 400 and 1000 fs, respectively. This step ensures that during NVT cooling, at no temperature point is there excessive free-volume or voids in the system which can cause inaccurate  $T_g$  results. We heat the system to 530 K in the NVT ensemble and gradually cool the system at 20 K increments back down to 210 K. At each temperature point, the mean squared displacement (MSD) of the system is calculated for 2 ns. Subsequently, the MSD in the subdiffusive regime is averaged and plotted versus the temperature. A characteristic slope change marking the transition from a glassy

behavior to rubbery behavior is identified as the  $T_g$ . The same protocol is used for all-atom simulations as well.

### 3. RESULTS AND DISCUSSION

In pursuit of establishing a universal coarse-grained (CG) force field for methacrylates, we first distinguish the parameters that are polymer chemistry specific versus parameters common to all methacrylates at the CG level. Our original assumption is that the number of terms for the bonded interactions of the polymer backbone can be reduced if the CG superatom locations are chosen to be consistent among all homopolymers studied. Thus, we first check the validity of this assumption by comparing the bonded distributions for bond stretching lengths, bending angles, and dihedral angles.

**3.1. Bonded Distribution Results.** A distinguishing feature of our modeling approach is that the backbone bead is assigned to be universal among all methacrylate-based monomer types to leverage the consistency in backbone structure. Additionally, we define the second bead to comprise the unique features of each monomer type, which is embodied in the distinctive side-chain. These two assumptions allow us to drastically reduce the number of parameters necessary to define the homopolymers. An additional benefit of this approach is that it is readily transferable to other monomers and can easily be used to study methacrylate copolymers as well, regardless of the sequence. To justify these assumptions, we have presented a thorough analysis of the probability distributions of the five homopolymers. These studies indicate that the backbone bonded interaction distributions are relatively similar across all five homopolymers, suggesting that a common set of parameters can be developed for these systems. These results are presented in Figure 2.

We find that the bond length distributions for AA and AB are similar regardless of homopolymer type and can be accurately described by a single set of Gaussian distribution parameters. (See Figure 2.) The resulting  $k$  value for the AA harmonic bond length potential is 105.0 kcal/mol. As a basis for relative comparison, a typical C–C bond energy is approximately 85 kcal/mol.<sup>42</sup> Note that these values cannot be directly compared due to discrepancies in effective bond definition and coarse grain bead masses. AB bond stretching lengths have a left-skewed probability distribution when plotted against bond distance, indicating a broader tail in short bond distances compared to longer distances. This is due to finite chain extensibility of the CCOC bonds in the methacrylate chain at longer lengths and the larger number of configurations available at shorter lengths. This results in a  $k$  value of 39.86 kcal/mol for the AB bond harmonic potential. Angle distributions for AAA and AAB are also similar among homopolymers. (See Figure 2.) The backbone distributions computed here have similar features as the one-bead and two-bead per monomer models that have recently been reported in the literature for p(MMA),<sup>12,36,37</sup> verifying that the common features are largely all-atom force-field independent. For example, we find that bond stretching AA and angle distributions AAA are similar compared to effective distributions from the previous one-bead per monomer study by Xia et al.<sup>12</sup> In addition, although our choice of bead centers is slightly different, we generate similar potential parameters to the two-bead CG model by Chen et al.<sup>37</sup> We note that in contrast to the latter study, we choose to base CG nonbonded potential parameters on  $T_g$  rather than on radial distribution functions, and we also use analytical potentials rather than tabular potentials to allow the model to

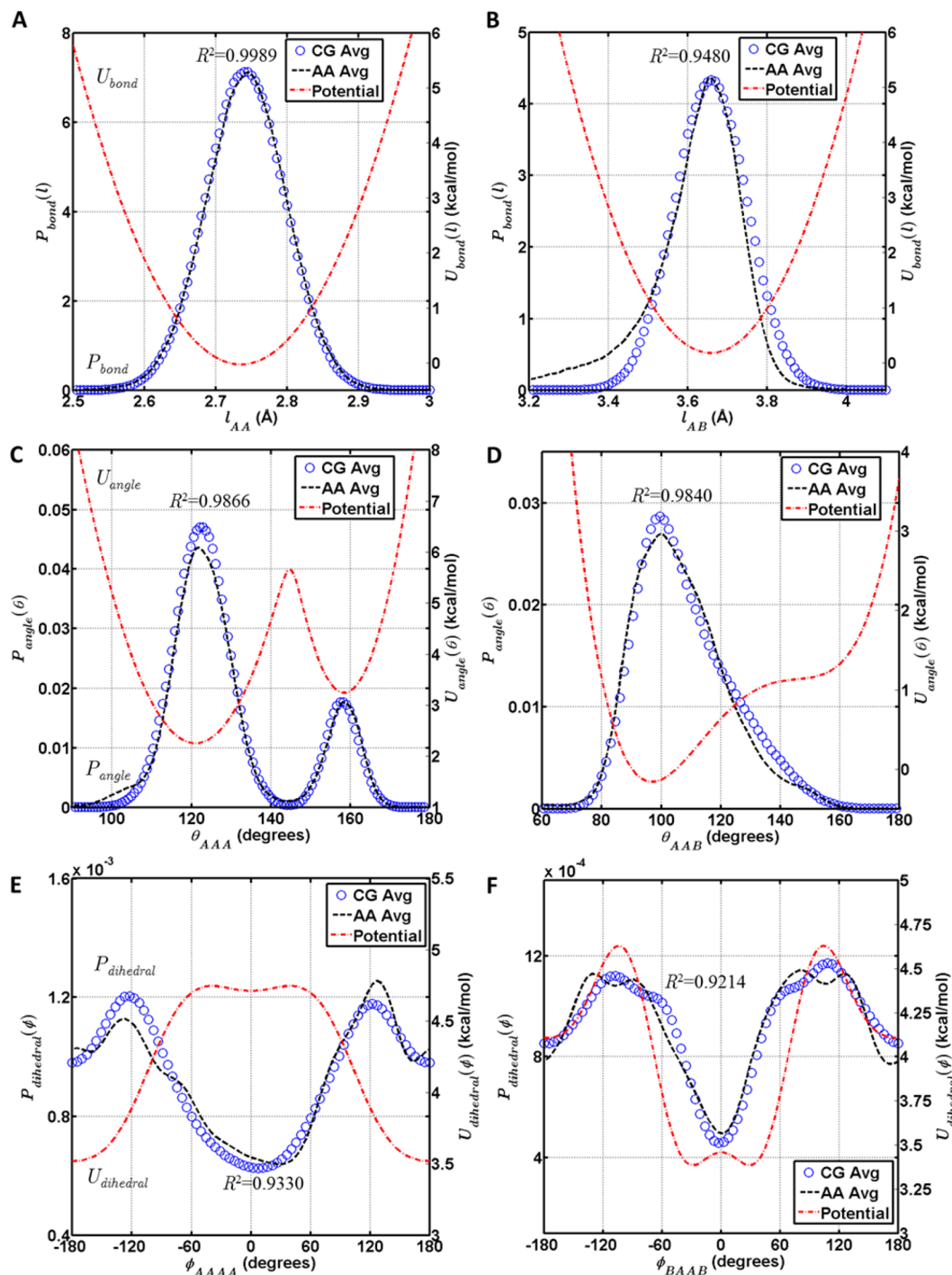


**Figure 3.** (A) Resulting coarse-grain backbone bond length distribution (A-A) for all polymers compared to the all-atomistic averaged distribution. (B) Backbone to adjacent side-chain bond length (A-B). (C) Backbone angle distribution (A-A-A). (D) Angle distribution between two adjacent backbone centers and a side-chain (A-A-B). (E) Backbone dihedral angle distribution (A-A-A-A). (F) Dihedral angle distribution for (B-A-A-B).

be easily transferred. Although dihedrals do show some variation across the homopolymer types, the similar features are prevalent enough for us to assume comparable dihedral correlation. Potential exceptions are the AAAA dihedral for p(HAMA) and p(MMA). The other three homopolymers indicate preference for +anticlinal and -anticlinal conformations along the backbone, while p(HAMA) favors the trans 180° state and p(MMA) has 0° favorability. This detail is averaged into the universal dihedral as an approximation. Overall, the similarities in bonded interactions across the five

monomer species confirm our hypothesis that consistent universal bonded potential terms can be developed for methacrylates.

Next, we demonstrate that the coarse-grain bonded distributions are able to reasonably match the target all-atomistic average distributions. The comparison between all-atomistic and coarse-grained models is measured using the coefficient of determination based on the ratio of the total squared residuals and the total sum of squares. This is similar to the merit function used in coarse-grained simplex optimization

**Table 1.** Functional Form of Force Field and Optimized Potential Parameters for the Universal Bonded Methacrylate Force Field

interaction	potential form	parameters
AA bond length	$U_{bondAA}(l) = k(l - l_0)^2$	$k = 105.0 \text{ kcal/mol}\cdot\text{\AA}^2, l_0 = 2.735 \text{ \AA}$
AB bond length	$U_{bondAB}(l) = k(l - l_0)^2$	$k = 39.86 \text{ kcal/mol}\cdot\text{\AA}^2, l_0 = 3.658 \text{ \AA}$
AAA angle	$U_{angleAAA}(\theta) = -k_b T \ln \left[ a_1 \exp \left( -\frac{\theta - \theta_1}{b_1} \right)^2 + a_2 \exp \left( -\frac{\theta - \theta_2}{b_2} \right)^2 \right]$	$a_1 = 2.294 \times 10^{-2}, b_1 = 9.493^\circ, \theta_1 = 121.0^\circ, a_2 = 4.367 \times 10^{-3}, b_2 = 6.210^\circ, \theta_2 = 158.5^\circ$
AAB angle	$U_{angleAAB}(\theta) = k_2(\theta - \theta_0)^2 + k_3(\theta - \theta_0)^3 + k_4(\theta - \theta_0)^4$	$k_2 = 9.881 \text{ kcal/mol}\cdot\text{rad}^2, k_3 = -15.12 \text{ kcal/mol}\cdot\text{rad}^3, k_4 = 6.589 \text{ kcal/mol}\cdot\text{rad}^4, \theta_0 = 1.690 \text{ rads}$
AAAA dihedral angle	$U_{dihedralAAAA}(\phi) = \sum_{k=1}^5 A_k \cos^{k-1}(\phi)$	$A_1 = 4.380 \text{ (kcal/mol)}, A_2 = 0.8739 \text{ (kcal/mol)}, A_3 = -0.3571 \text{ (kcal/mol)}, A_4 = -0.2774 \text{ (kcal/mol)}, A_5 = 0.09312 \text{ (kcal/mol)}$
BAAB dihedral angle	$U_{dihedralBAAB}(\phi) = \sum_{k=1}^5 A_k \cos^{k-1}(\phi)$	$A_1 = 4.519 \text{ (kcal/mol)}, A_2 = -0.8859 \text{ (kcal/mol)}, A_3 = -1.692 \text{ (kcal/mol)}, A_4 = 0.5625 \text{ (kcal/mol)}, A_5 = 0.9562 \text{ (kcal/mol)}$
nonbonded	$U_{nonbond} = 4\epsilon \left[ \left( \frac{\sigma}{r} \right)^{12} - \left( \frac{\sigma}{r} \right)^6 \right] + S_{LJ}(r)$	(See Table 2)

**Table 2.** Nonbonded 12-6 LJ Potential Parameters Tuned To Match Atomistic Density and Glass Transition

monomer	$\epsilon_{AA}$ (kcal/mol)	$\sigma_{AA}$ (Angs)	$\epsilon_{BB}$ (kcal/mol)	$\sigma_{BB}$ (Angs)	$\epsilon_{AB}$ (kcal/mol)	$\sigma_{AB}$ (Angs)
p(ECPMA)	0.500	5.500	0.475	6.570	0.487	6.035
p(aGBLMA)	0.500	5.500	1.100	5.520	0.742	5.510
p(HAMA)	0.500	5.500	2.450	6.730	3.500	6.115
p(MAMA)	0.500	5.500	1.100	7.090	0.742	6.295
p(MMA)	0.500	5.500	1.500	4.420	0.866	4.960

**Table 3.**  $T_g$  and Density for Each p(ECPMA), p(aGBLMA), p(HAMA), and p(MAMA) for All-Atom and Coarse-Grain Monomer Simulations at 300 K

monomer	monomer weight (g/mol)	all-atomistic $T_g$ (K)	coarse-grain $T_g$ (K)	all-atomistic $\rho$ (g/cm <sup>3</sup> )	coarse-grain $\rho$ (g/cm <sup>3</sup> )
p(ECPMA)	184	$334.3 \pm 24.1$	$333.6 \pm 7.4$	0.987	0.988
p(aGBLMA)	172	$393.8 \pm 13.5$	$402.1 \pm 5.9$	1.316	1.321
p(HAMA)	238	$467.2 \pm 14.0$	$460.0 \pm 9.7$	1.133	1.133
p(MAMA)	236	$430.1 \pm 6.5$	$441.0 \pm 4.5$	0.965	0.974
p(MMA)	102	$395.6 \pm 11.9$	$385.2 \pm 1.9$	1.113	1.147

studies.<sup>39</sup> We follow the IBM procedure outlined in the previous methods section to optimize the CG average bonded distributions with the all-atom average distributions. After about 10 Boltzmann iterations, CG distributions for AA and AB bond lengths are shown to be very consistent with all-atomistic distributions with  $R^2 = 0.9989$  and 0.9480, respectively. (See Figures 3A and 3B.) We employ simple analytical coarse-grain potentials to reproduce the target all-atomistic average bond length distributions.

For AAA angles, each polymer type shows a similar double peak distribution with a larger maximum at  $\sim 120^\circ$  and a smaller maximum at  $\sim 160^\circ$ . The average overall distributions (black dotted line) are first fit with an analytical double Gaussian equation and are then inverted using the Inverse Boltzmann Method. The CG potential is optimized using the Iterative Boltzmann Method with the dihedral and nonbonded interactions turned off. The CG potential is implemented in LAMMPS using the tabulated data from the analytical equation. The final distributions with the full force-field turned on are shown in Figure 3C and have  $R^2 = 0.9866$  between the CG and all-atom distributions.

AAB angles approximate a Gaussian distribution with slight right-skewness. AAB angles are defined as both the forward and backward angles between two adjacent backbone beads and a

connected side-chain bead. The favored angle is about  $\sim 105^\circ$ . The target all-atomistic average distribution is fit and optimized with a quadratic function using 12 iterations. The optimization is performed without nonbonded or dihedral potentials. The AAB CG distributions with the full force field are displayed in Figure 3D with  $R^2 = 0.9840$ .

Finally, we demonstrate that CG dihedral angles can be optimized to fit the all-atomistic average distribution with  $R^2 = 0.9330$ . Averaged dihedral distributions for AAAA dihedrals show that the favored conformation is +anticlinal and -anticlinal at  $+120$  and  $-120^\circ$ . After 12 iterations, the final distribution comparison is shown in Figure 3E with the full force field.

BAAB dihedral angles also prefer +anticlinal and -anticlinal conformations, while the preferred position of the maxima is broadened due to the average over the five homopolymer types. This configuration is highly preferred from the angle and nonbonded interactions even without explicit dihedral interactions. This results in a dihedral potential which appears atypical because it is used to improve the overall fit to the all-atomistic average rather than to drive the distribution. Optimization after 12 iterations is shown in Figure 3F with the full force field.  $R^2 = 0.9214$  between the CG and all-atom distributions. The parameters and analytical potentials for

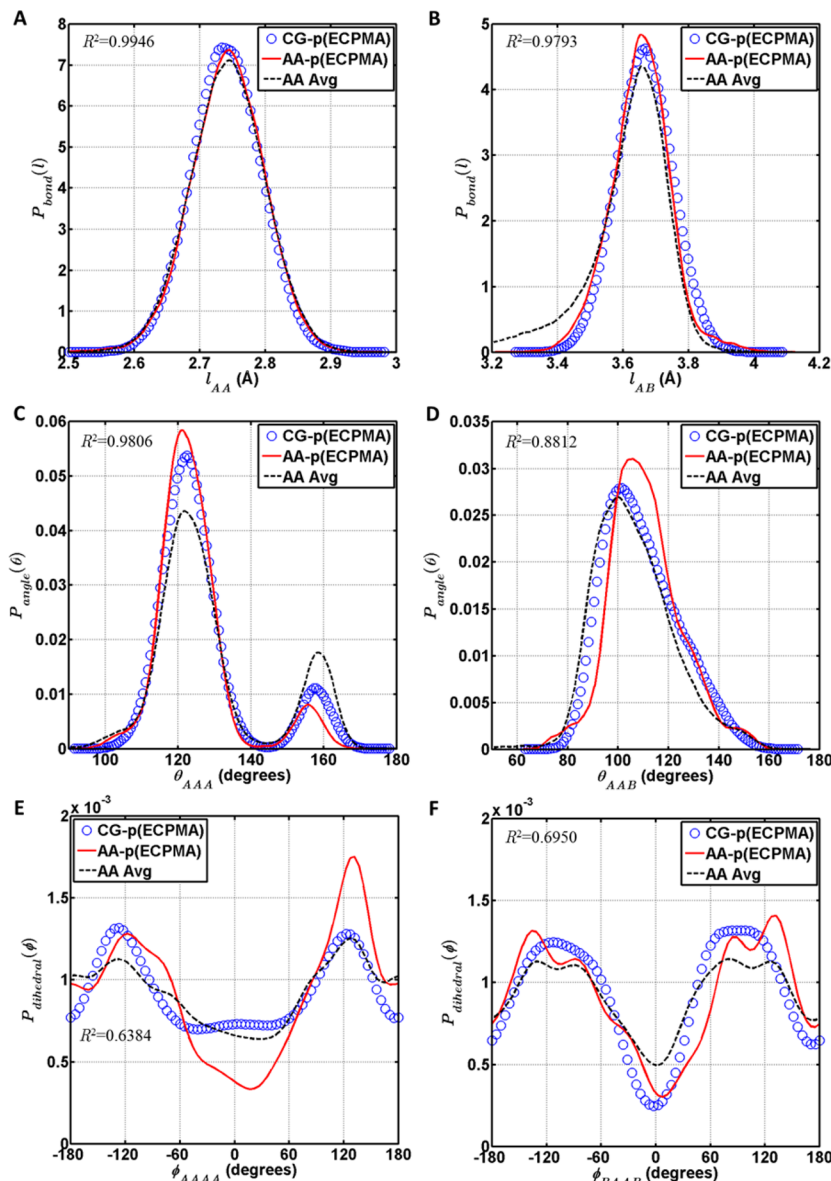


**Figure 4.** Comparison of bonded interactions coarse-grain versus all-atomistic distributions for p(ECPMA). (A) (A-A) bond length, (B) (A-B) bond length, (C) (A-A-A) backbone angle, (D) (A-A-B) backbone to side-chain angle, (E) (A-A-A-A) backbone dihedral, (F) (B-A-A-B) side-chain to backbone dihedral.

bonded interactions are shown in Table 1. The parameters for nonbonded interactions are shown in Table 2, and the resulting comparison of  $T_g$  and density between all-atom and coarse-grain models is shown in Table 3.

**3.2. Density and  $T_g$  Results.** In order to determine the coarse-grained nonbonded potential parameters, we systematically vary the  $\sigma$  and  $\epsilon$  of the Lennard-Jones potential to tune the model properties to the all-atomistic density and  $T_g$ . Typically, due to the reduction of degrees of freedom in the CG description, the effective friction and caging effects on polymer chains are reduced. This causes dynamic phenomena such as diffusion to occur more rapidly in CG simulations than in all-atomistic simulations, which also gives rise to lower elastic constants.<sup>22,36,38,43,44</sup> The loss of intermolecular friction is often reintroduced into the system through various approaches, for instance, by changing the equations of motion with a dissipative particle dynamics or Lowe-Andersen thermostat.<sup>43,45</sup> In our case, we find that tuning the system friction is not sufficient in

capturing the all-atom  $T_g$  consistently. This is likely due to the property dependence on not only the system dynamics but also the structural confinement of chains, which is also altered during the coarsening step. We therefore tune pairwise interactions in order to match the CG  $T_g$  value to the all-atom  $T_g$  value. This approach was shown to be effective in our earlier studies with simpler one-bead CG models.<sup>12,13</sup> We find that while the  $\sigma$  value does have an effect on both the density and  $T_g$  of the system as it changes polymer excluded volume and system free-volume,  $\epsilon$  does not have a strong effect on the density over small variations. Hence, we choose to tune the  $\sigma$  value first to match the atomistic density, and then tune the  $\epsilon$  value to match the  $T_g$ . The resulting nonbonded potential parameters and property comparisons are shown in Table 2 and Table 3, respectively. We find that the results of the tunable parameters correspond well with the physical structure of each homopolymer. For instance, the side-chain group physical volume generally scales similarly to the resulting  $\sigma_{BB}$  values,

where the p(MMA) side-chain occupies the smallest volume, and therefore also has the smallest  $\sigma_{BB}$ . Likewise, p(HAMA) and p(MAMA) have the largest side-chain groups and correspondingly, have the largest  $\sigma_{BB}$  values. The  $\epsilon_{BB}$  ranking from lowest to highest values generally corresponds with the rank of  $T_g$  for each homopolymer. P(MMA) may be an exception due to the small size of the side-chain group, which requires higher effective interactions to replicate packing of the atomistic structure. Resulting  $\epsilon_{AA}$  and  $\epsilon_{BB}$  values (0.45–1.5 kcal/mol for non-hydrogen bonding species) are reasonable given that typical van der Waals energies range from 0.5 to 1.0 kcal/mol per atom pair, and CG bead interactions represent a mean-field effect of multiple atoms.<sup>42</sup>

Among the small sample size of homopolymer species, there is a diverse set of side-chain chemistries. For example, p(HAMA) has hydrogen bonding functionality, p(aGBLMA) has a polar side-chain, and p(MMA), p(ECPMA), and p(MAMA) have nonpolar side-chain groups with varying bulkiness. In general,  $\epsilon_{BB}$  correlates with the strength of the chemical interaction, but there are notable differences due to packing efficiency and size of the group. Variations in side-chain group bulkiness and flexibility also affect the conformational mobility of the chain, packing efficiency, and thus,  $T_g$ .

Once the optimization of the averaged CG potentials provide bonded distributions in good agreement with the averaged all-atomistic distributions, a comparison between the nonaveraged individual homopolymers is also performed. As a representative case, results for p(ECPMA) are shown in Figure 4. Even though the CG model is calibrated for average distributions, at the individual homopolymer level, there is strong correlation between the CG and all-atom distributions ( $R^2$  values are reported in Figure 4). Each homopolymer all-atom distribution features peaks that are slightly higher or lower than the averaged distribution, which is expected due to differences in the relative side-chain excluded volume and mass.<sup>46</sup> The associated CG distribution typically follows the same trend in variation, but some minor differences can be noted particularly for lower energy contributions such as dihedrals. In the case of p(ECPMA), the all-atom distribution for BAAB dihedrals shows symmetry about the 0° axis with local peaks at the +anticlinal and –anticlinal angles. This profile is influenced by the asymmetric side-chain, which is able to rotate about the connecting bond to the methacrylate oxygen, which is a feature that is lost when converting to a symmetrical, spherical side-chain bead and is reflected in the lower  $R^2$  value. (See Figure 4F.)

**3.3. Coarse-Grain Model Validations.** We validate the coarse-grain model by comparing the glass transition dependence on molecular weight with the all-atomistic results according to the Flory–Fox equation. This equation quantifies the dependence of  $T_g$  on molecular weight:  $T_g(M_n) = T_{g\infty} - K/M_n$ , where  $T_{g\infty}$  is the converged glass transition temperature as the degree of polymerization approaches infinity. To this end, we generate four different chain length systems, of degree of polymerization, DPn = 20, 50, 100, and 200. We vary the number of chains per simulation case to ensure that we have the same number of beads (20,000) for each simulation and utilize the same  $T_g$  estimation method described in the previous methods section, over 5 replicas per case to improve statistics. We find that the Flory–Fox fitting equation is in very good agreement with the all-atomistic results, where the all-atomistic Flory–Fox curve remains within one standard deviation of the mean simulated CG values. (See Figure 5.) This analysis is

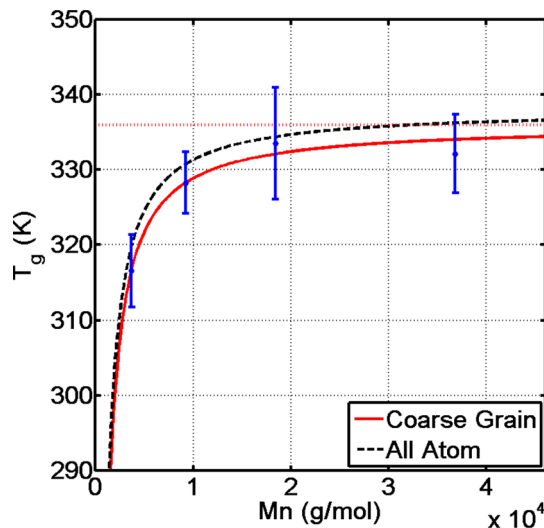


**Figure 5.** Flory–Fox equation fit for coarse-grain simulations versus all-atomistic results for p(ECPMA). The molecular weight dependence on  $T_g$  from 20 to 400 monomers per chain shows good agreement with the atomistic Flory–Fox results.

performed for p(ECPMA) only because the  $T_g$  elevation due to an increase in the DPn from 20 to 200 is indiscernible (i.e., within simulation error) for most of the other homopolymer systems. This is due to the high  $T_g$  of these specialized homopolymers at even very low molecular weights ( $M_w$ ), which allows their  $T_g$  to be tailored in co and ter-polymer photoresist thin film applications.

The above results illustrate that glass transition temperature can be well matched by CG models. To probe further into the dynamics of the all-atom and CG models, we quantify the self-diffusion behavior in the liquid monomer state to get a sense of the pure dynamics scaling of the CG model versus the all-atomistic system. In most multiscale approaches, a large discrepancy between the dynamics of a CG model compared to its all-atomistic counterpart is expected due to lost-degrees of freedom and reduced intermolecular friction that hinders diffusion and cooperative segmental mobility. In our case, instead of matching the nonbonded interactions to the structural RDF, we choose to tune the  $\sigma$  and  $\epsilon$  values of the 12–6 Lennard-Jones potential to match the density and  $T_g$  of the all-atomistic simulation. By increasing  $\epsilon$ , the Lennard-Jones well depth, we essentially increase the energy cost for neighboring nonbonded CG beads to move away from their equilibrium spacing, which increases the temperature required for the beads to exit their vitrified positions. Although this method does slow down the dynamics of the system drastically, it does not certify that the resulting dynamics of the CG model will be comparable to all-atomistic dynamics.<sup>47</sup> In this study, we find that the dynamics of the CG models developed are slower than each corresponding all-atom system but remarkably are in the same order of magnitude for the five homopolymers. (See Figure 6.) In the case of HAMA monomers, we systematically varied the  $\epsilon_{AB}$  value to account for hydrogen bonding. By increasing the  $\epsilon_{AB}$  to 3.5 kcal/mol for HAMA, we find that we can reasonably match both the  $T_g$  and the self-diffusion coefficient of the all-atom simulations. We take this to be a mean field approximation of the increased backbone-side-chain interaction energy, as there is no directionality associated with the LJ potential in the CG model. We note that the resulting  $\epsilon_{AB}$  value is in agreement with effective monomer interactions

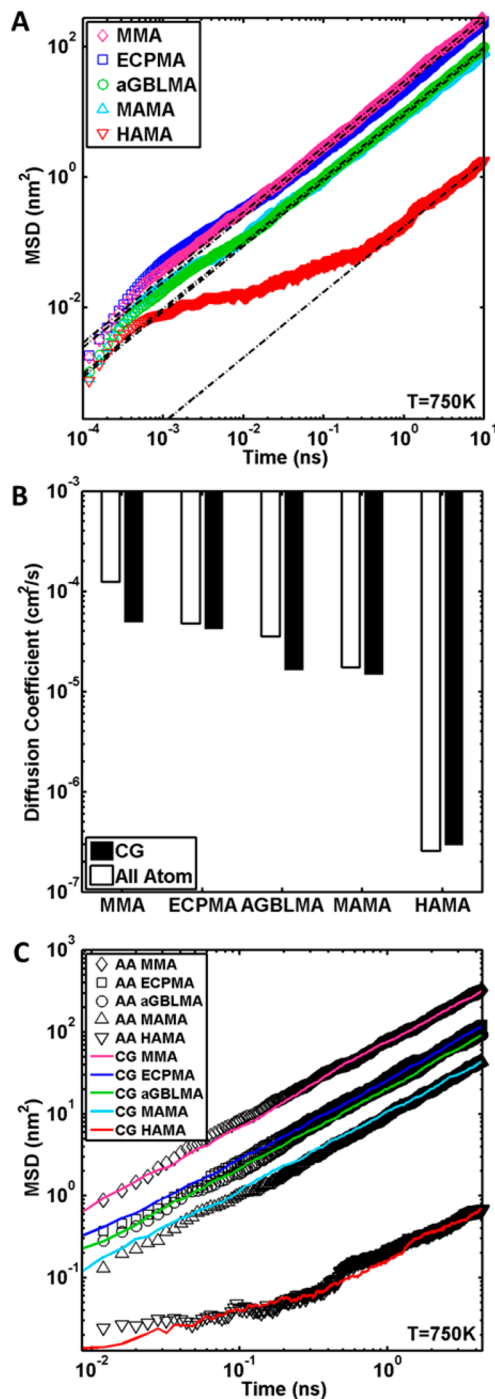


**Figure 6.** (A) Log–log plot of unscaled liquid monomer MSD vs time for MMA, ECPMA, aGBLMA, MAMA, and HAMA coarse-grain models over 10 ns. Dash-dotted lines show linear scaling with  $t$ . (B) Unscaled diffusion coefficient for all-atomistic and coarse-grain liquid monomer systems at 750 K. (C) MSD vs time for MMA, ECPMA, aGBLMA, MAMA, and HAMA monomers after scaling the CG model to all-atom simulations according to the scaling factors in Table 4.

involving hydrogen bonds, which are weak interactions with energies in the range of 1.2 to 7.2 kcal/mol.<sup>42</sup> The fact that the dynamics occur in roughly the same order of magnitude in terms of time-scales suggests that the interactions we have chosen to match the  $T_g$  of the polymers also alleviate for the loss of friction that is commonly observed in purely structure-based CG approaches. We also point out that the polarity and

hydrogen bonding effects on  $T_g$  and dynamic behavior are able to be reproduced by the Lennard-Jones pairwise potential and without explicit charge or hydrogen-bonding terms in the coarse-grain model.

To more precisely match dynamic quantities computed in all-atom and CG systems, it is common to use scaling relationships. Harmandaris and Kremer<sup>17</sup> suggest that a time scaling factor,  $S_{AA-CG}$ , can be used to correct for the discrepancy in the dynamics of the CG system. This factor is dependent on polymer chain length,  $M$ , and can be defined by the ratio of effective friction  $\zeta$  in the CG vs atomistic system, namely,  $(S_{AA-CG}(M)) = \zeta^{AA}/\zeta^{CG}$ . This quantity is the same as the CG vs all-atom simulated self-diffusion ratio and is unique for each homopolymer system and molecular weight.<sup>21</sup> Here, using the same approach, we scale the MSD vs time curves for the CG models to the all-atomistic curves using different factors for each homopolymer based on the ratio of the CG and all-atom self-diffusion coefficients. The resulting curves show good correlation between CG and all-atom models for MMA, ECPMA, aGBLMA, and MAMA liquid monomer diffusion. HAMA CG and all-atom curves show deviation at shorter, transient time scales but do correlate in the nanosecond time scale region. (See Figure 6.) The unscaled diffusion coefficients are reported in Table 4 for comparison as well as in Figure 6B.

**Table 4. Diffusion Coefficient for Each ECPMA, aGBLMA, HAMA, and MAMA for All-Atom and Coarse-Grain Liquid Monomer Simulations at 750 K**

monomer	all-atom self-diffusion coefficient (cm²/s)	coarse-grain self-diffusion coefficient (cm²/s)	monomer scaling factor $S_{AA-CG}$
ECPMA	$4.76 \times 10^{-05}$	$4.15 \times 10^{-05}$	1.1
aGBLMA	$3.52 \times 10^{-05}$	$1.63 \times 10^{-05}$	2.2
HAMA	$2.54 \times 10^{-07}$	$2.90 \times 10^{-07}$	0.88
MAMA	$1.73 \times 10^{-05}$	$1.46 \times 10^{-05}$	1.2
MMA	$1.24 \times 10^{-04}$	$4.88 \times 10^{-05}$	2.5

Overall, these results suggest that the key dynamic properties of the all-atom systems can be reproduced with the generic, transferable two-bead modeling strategy presented in this paper. Most notably, the CG models rank the diffusion constant, glass-transition temperature and density of the specific homopolymers in correct order without the need for an excessive number of parameters. The CG model reduces the number of degrees of freedom and does not require complex interaction terms. When combined with using a larger time step and simple analytical potentials, the CG model can achieve a speed-up many times faster than the all-atomistic model. We employ a simulation efficiency factor for each system equal to the number of effective atoms multiplied by the ratio of simulation-time to CPU-time. For example, on the basis of a 300 monomer bulk p(MMA) system which has the lowest average atom to CG bead ratio (8:1), we find that the minimum speed-up for the CG model is nearly 150 times faster. In the case of p(MAMA), which has the largest average atom to CG bead ratio (20:1) for the side-chain, we find that the CG model is over 700 times faster than the all-atomistic model.

Finally, we evaluate the mechanical properties of the resulting CG model by stretching bulk p(MMA) in the elastic regime while measuring the stress. (See Figure 7.) The starting system contains 100 chains each with 100 repeat units. We stretch the system at  $5 \times 10^8$  s<sup>-1</sup> strain rate at a temperature of 300 K and measure the tensile modulus of elasticity to be the

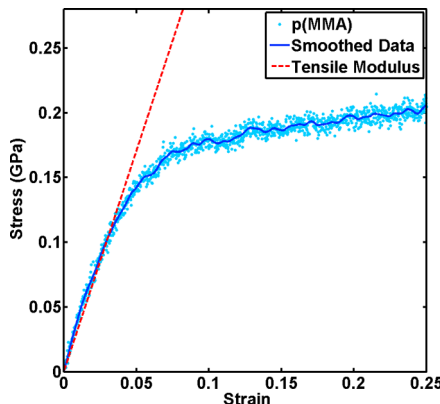


**Figure 7.** Stress vs strain curve for coarse-grain bulk p(MMA) to 25% engineering strain. Dotted line shows the elastic modulus taken as the slope from 0% to 4% strain.

initial slope of the stress strain curve from 0 to 4% strain. Although the strain rate is significantly higher than experimental pulling rates, the modulus of p(MMA) in the glassy state does not increase appreciably at rates above  $10^4 \text{ s}^{-1}$  according to experimental studies.<sup>48</sup> We find that the average elastic modulus is 3.4 GPa with a standard deviation of 0.051 GPa, which correlates well with experimental results (3.3 GPa).<sup>49</sup> We restrict our analysis to p(MMA) because we do not have experimental data for comparison for the other specialized homopolymers. These results, while somewhat preliminary, illustrate that matching dynamic properties such as  $T_g$  at the coarse-scale can be an effective way to reproduce mechanical properties more accurately in the linear elastic range. Our CG methodology may lay the foundation for future studies aimed at capturing mechanical properties at extended length and time scales for a broader range of polymer systems.

#### 4. CONCLUSIONS

We have presented a systematic methodology for generating a thermomechanically consistent coarse-grain model and have applied it to establish the universal parameters for methacrylate-based polymers. The appealing transferable features of this CG model arises from the choice of the locations for coarse-grain bead centers, as well as by leveraging the common backbone structure across the methacrylate monomers chosen, which gives rise to universal bonded and nonbonded parameters along the consistent backbone. The all-atomistic bonded distributions for each homopolymer system show similar trends and can be fitted with simple analytical functions. We use the Iterative Boltzmann Method to optimize the averaged CG bonded potential terms to match the target all-atomistic average distributions starting from the highest energy contributing bond-length interaction to the lowest energy contributing dihedral angles. Simply customizing the nonbonded parameters and masses for the side-chain beads captures certain unique monomer characteristics. We find that this method can be used to tune the model to precisely match the density and glass transition behavior of each of the atomistic homopolymer models without explicit charge or hydrogen bonding terms. We verify the validity of the model by demonstrating that the Flory–Fox fitting constants of the molecular weight dependent  $T_g$  are well correlated between the all-atomistic and coarse-grained simulations. Additionally, elastic constants of the CG

model obtained for p(MMA) match experimental values for this system.

The key contributions of our methodology and its significance can be summarized as follows. First, by decreasing the number of degrees of freedom and using simple analytical potentials, we are able to achieve a CG model that can run 150 to 700 times faster than the all-atomistic model, for example, on the basis of a 300 monomer methacrylate system. Second, by choosing common methacrylate monomers as a focus group of tremendous importance in polymer science, we provide a convincing approach for establishing transferable CG models for subclasses of polymers that have common backbone features and diverse material properties arising from side-chain functionality. The simultaneous prediction of this set of structural, dynamic, and thermomechanical objectives has not been previously achieved with CG models of engineering polymers that typically are parametrized for a single homopolymer. Third, the comparative nature of the methodology identifies universal backbone attributes of a range of methacrylate monomers and is readily applicable to copolymer systems without the need to introduce new interface bonded parameters due to our universal definition of backbone and side-chain force centers and potential terms. The versatility of our model makes it particularly useful for the design of nanoelectronics, nanocomposites and thin films based on copolymer materials where sequence and composition effects remain to be fully understood and cannot be easily probed with all-atom simulations or experiments.

#### ■ AUTHOR INFORMATION

##### Corresponding Author

\*Phone: 847-491-5282. E-mail: s-keten@northwestern.edu. Corresponding author address: Dept. of Civil & Environmental Engineering and Dept. of Mechanical Engineering, Room A133, Northwestern University, 2145 Sheridan Road, Evanston, IL 60208-3109.

##### Author Contributions

The manuscript was written through contributions of all authors. All authors have given approval to the final version of the manuscript.

##### Notes

The authors declare no competing financial interest.

#### ■ ACKNOWLEDGMENTS

D.H., W.X., S.A., and S.K. acknowledge support by the University Partnership Initiative between Northwestern University and The Dow Chemical Company and from the Dept. of Civil & Environmental Engineering and Mechanical Engineering at Northwestern University. A supercomputing grant from Quest HPC System at Northwestern University is also acknowledged.

#### ■ REFERENCES

- (1) Abraham, J. K.; Philip, B.; Witchurch, A.; Varadan, V. K.; Reddy, C. C. A compact wireless gas sensor using a carbon nanotube/PMMA thin film chemiresistor. *Smart Mater. Struct.* **2004**, *13* (5), 1045–1049.
- (2) Ash, B. J.; Siegel, R. W.; Schadler, L. S. Glass-transition temperature behavior of alumina/PMMA nanocomposites. *J. Polym. Sci., Polym. Phys.* **2004**, *42* (23), 4371–4383.
- (3) Avella, M.; Errico, M. E.; Martuscelli, E. Novel PMMA/CaCO<sub>3</sub> nanocomposites abrasion resistant prepared by an in situ polymerization process. *Nano Lett.* **2001**, *1* (4), 213–217.

- (4) Fasolka, M. J.; Mayes, A. M. Block copolymer thin films: Physics and applications. *Annu. Rev. Mater. Res.* **2001**, *31*, 323–355.
- (5) Richard, A. Interface and surface effects on the glass-transition temperature in thin polymer films. *Faraday Discuss.* **1994**, *98*, 219–230.
- (6) Lee, L.-H.; Chen, W.-C. High-refractive-index thin films prepared from trialkoxysilane-capped poly (methyl methacrylate)-titania materials. *Chem. Mater.* **2001**, *13* (3), 1137–1142.
- (7) Shin, H. S.; Jung, Y. M.; Oh, T. Y.; Chang, T.; Kim, S. B.; Lee, D. H.; Noda, I. Glass transition temperature and conformational changes of poly (methyl methacrylate) thin films determined by a two-dimensional map representation of temperature-dependent reflection-absorption FTIR spectra. *Langmuir* **2002**, *18* (15), 5953–5958.
- (8) Limm, W.; Winnik, M. A.; Smith, B. A. Photochemical free-volume generation in poly (methyl methacrylate) photoresists. *Polym. Eng. Sci.* **1989**, *29* (14), 911–915.
- (9) Fouchier, M.; Pargon, E.; Azarnouche, L.; Menguelti, K.; Joubert, O.; Cardolaccia, T.; Bae, Y. C. Vacuum ultra violet absorption spectroscopy of 193 nm photoresists. *Appl. Phys. A: Mater. Sci. Process.* **2011**, *105* (2), 399–405.
- (10) Philip, B.; Abraham, J. K.; Chandrasekhar, A.; Varadan, V. K. Carbon nanotube/PMMA composite thin films for gas-sensing applications. *Smart Mater. Struct.* **2003**, *12* (6), 935–939.
- (11) Morita, H.; Tanaka, K.; Kajiyama, T.; Nishi, T.; Doi, M. Study of the glass transition temperature of polymer surface by coarse-grained molecular dynamics simulation. *Macromolecules* **2006**, *39* (18), 6233–6237.
- (12) Xia, W.; Mishra, S.; Keten, S. Substrate vs. Free Surface: Competing Effects on the Glass Transition of Polymer Thin Films. *Polymer* **2013**, *54* (21), 5942–5951.
- (13) Xia, W.; Keten, S. Coupled Effects of the Substrate Adhesion and Intermolecular Forces on Polymer Thin Film Glass-Transition Behavior. *Langmuir* **2013**, *29* (41), 12730–12736.
- (14) Pike, D. Q.; Detcheverry, F. A.; Muller, M.; de Pablo, J. J. Theoretically informed coarse grain simulations of polymeric systems. *J. Chem. Phys.* **2009**, *131* (8), 084903–1–084903–10.
- (15) Sun, Q.; Faller, R. Systematic coarse-graining of a polymer blend: Polyisoprene and polystyrene. *J. Chem. Theory Comput.* **2006**, *2* (3), 607–615.
- (16) Wu, C. Simulated Glass Transition of Poly (ethylene oxide) Bulk and Film: A Comparative Study. *J. Phys. Chem. B* **2011**, *115* (38), 11044–11052.
- (17) Muller-Plathe, F. Coarse-graining in polymer simulation: from the atomistic to the mesoscopic scale and back. *ChemPhysChem* **2002**, *3* (9), 755–769.
- (18) Nielsen, S. O.; Lopez, C. F.; Srinivas, G.; Klein, M. L. Coarse grain models and the computer simulation of soft materials. *J. Phys.: Condens. Matter* **2004**, *16* (15), R481–R512.
- (19) Voth, G. A. *Coarse-graining of condensed phase and biomolecular systems*; CRC Press: Boca Raton, 2009; p xviii, 455 p., 16 p. of plates.
- (20) Harmandaris, V. A.; Adhikari, N. P.; van der Vegt, N. F. A.; Kremer, K. Hierarchical modeling of polystyrene: From atomistic to coarse-grained simulations. *Macromolecules* **2006**, *39* (19), 6708–6719.
- (21) Harmandaris, V. A.; Reith, D.; Van der Vegt, N. F. A.; Kremer, K. Comparison between coarse-graining models for polymer systems: Two mapping schemes for polystyrene. *Macromol. Chem. Phys.* **2007**, *208* (19–20), 2109–2120.
- (22) Harmandaris, V. A.; Kremer, K. Dynamics of Polystyrene Melts through Hierarchical Multiscale Simulations. *Macromolecules* **2009**, *42* (3), 791–802.
- (23) Fritz, D.; Harmandaris, V. A.; Kremer, K.; van der Vegt, N. F. A. Coarse-Grained Polymer Melts Based on Isolated Atomistic Chains: Simulation of Polystyrene of Different Tacticities. *Macromolecules* **2009**, *42* (19), 7579–7588.
- (24) Noid, W. G.; Chu, J. W.; Ayton, G. S.; Krishna, V.; Izvekov, S.; Voth, G. A.; Das, A.; Andersen, H. C. The multiscale coarse-graining method. I. A rigorous bridge between atomistic and coarse-grained models. *J. Chem. Phys.* **2008**, *128* (24), 244114–1–244114–11.
- (25) Marrink, S. J.; Risselada, H. J.; Yefimov, S.; Tieleman, D. P.; de Vries, A. H. The MARTINI force field: Coarse grained model for biomolecular simulations. *J. Phys. Chem. B* **2007**, *111* (27), 7812–7824.
- (26) Monticelli, L.; Kandasamy, S. K.; Periole, X.; Larson, R. G.; Tieleman, D. P.; Marrink, S. J. The MARTINI coarse-grained force field: Extension to proteins. *J. Chem. Theory Comput.* **2008**, *4* (5), 819–834.
- (27) Anderson, J. A.; Travesset, A. Coarse-grained simulations of gels of nonionic multiblock copolymers with hydrophobic groups. *Macromolecules* **2006**, *39* (15), 5143–5151.
- (28) Li, X. J.; Kou, D. Z.; Rao, S. L.; Liang, H. J. Developing a coarse-grained force field for the diblock copolymer poly(styrene-b-butadiene) from atomistic simulation. *J. Chem. Phys.* **2006**, *124* (20), 204909–1–204909–7.
- (29) Srinivas, G.; Discher, D. E.; Klein, M. L. Self-assembly and properties of diblock copolymers by coarse-grain molecular dynamics. *Nat. Mater.* **2004**, *3* (9), 638–644.
- (30) Srinivas, G.; Shelley, J. C.; Nielsen, S. O.; Discher, D. E.; Klein, M. L. Simulation of diblock copolymer self-assembly, using a coarse-grain model. *J. Phys. Chem. B* **2004**, *108* (24), 8153–8160.
- (31) Rolfe, B. A.; Chun, J.; Joo, Y. L. Dynamics of micelle-nanoparticle systems undergoing shear: a coarse-grained molecular dynamics approach. *Soft Matter* **2013**, *9* (43), 10294–10305.
- (32) Plimpton, S.; Crozier, P.; Thompson, A. *LAMMPS-large-scale atomic/molecular massively parallel simulator*; Sandia National Laboratories: 2007.
- (33) Mayo, S. L.; Olafson, B. D.; Goddard, W. A. Dreiding - a Generic Force-Field for Molecular Simulations. *J. Phys. Chem.* **1990**, *94* (26), 8897–8909.
- (34) Payne, M. C.; Teter, M. P.; Allan, D. C.; Arias, T. A.; Joannopoulos, J. D. Iterative Minimization Techniques for Ab initio Total-Energy Calculations - Molecular-Dynamics and Conjugate Gradients. *Rev. Mod. Phys.* **1992**, *64* (4), 1045–1097.
- (35) Faller, R. Automatic coarse graining of polymers. *Polymer* **2004**, *45* (11), 3869–3876.
- (36) Depa, P.; Chen, C.; Maranas, J. K. Why are coarse-grained force fields too fast? A look at dynamics of four coarse-grained polymers. *J. Chem. Phys.* **2011**, *134*, 014903–1–014903–8.
- (37) Chen, C. X.; Depa, P.; Maranas, J. K.; Sakai, V. G. Comparison of explicit atom, united atom, and coarse-grained simulations of poly(methyl methacrylate). *J. Chem. Phys.* **2008**, *128* (12), 124906–1–124906–12.
- (38) Akkermans, R. L. C.; Briels, W. J. A structure-based coarse-grained model for polymer melts. *J. Chem. Phys.* **2001**, *114* (2), 1020–1031.
- (39) Reith, D.; Meyer, H.; Muller-Plathe, F. Mapping atomistic to coarse-grained polymer models using automatic simplex optimization to fit structural properties. *Macromolecules* **2001**, *34* (7), 2335–2345.
- (40) Dixon, W. J. Efficient analysis of experimental observations. *Annu. Rev. Pharmacol. Toxicol.* **1980**, *20* (1), 441–462.
- (41) Tsige, M.; Taylor, P. L. Simulation study of the glass transition temperature in poly(methyl methacrylate). *Phys. Rev. E* **2002**, *65* (2), 021805–1–021805–8.
- (42) Berg, J. M.; Tymoczko, J. L.; Stryer, L. *Biochemistry*; W. H. Freeman and Company: New York, 2002.
- (43) Qian, H.-J.; Liew, C. C.; Müller-Plathe, F. Effective control of the transport coefficients of a coarse-grained liquid and polymer models using the dissipative particle dynamics and Lowe–Andersen equations of motion. *Phys. Chem. Chem. Phys.* **2009**, *11* (12), 1962–1969.
- (44) Izvekov, S.; Voth, G. A. A multiscale coarse-graining method for biomolecular systems. *J. Phys. Chem. B* **2005**, *109* (7), 2469–2473.
- (45) Fu, C.-C.; Kulkarni, P. M.; Shell, M. S.; Leal, L. G. A test of systematic coarse-graining of molecular dynamics simulations: Transport properties. *J. Chem. Phys.* **2013**, *139*, 094107–1–094107–12.
- (46) Abrams, C. F.; Kremer, K. Combined coarse-grained and atomistic simulation of liquid bisphenol A-polycarbonate: Liquid

packing and intramolecular structure. *Macromolecules* **2003**, *36* (1), 260–267.

(47) Akkermans, R. L. C.; Briels, W. J. Coarse-grained dynamics of one chain in a polymer melt. *J. Chem. Phys.* **2000**, *113* (15), 6409–6422.

(48) Mulliken, A. D.; Boyce, M. C. Mechanics of the rate-dependent elastic-plastic deformation of glassy polymers from low to high strain rates. *Int. J. Solids. Struct.* **2006**, *43* (5), 1331–1356.

(49) Brandrup, J.; Immergut, E. H.; Grulke, E. A. *Polymer Handbook*, 4th ed.; Wiley: New York, 1999.